

Transesterification Thio Effects of Phosphate Diesters: Free Energy Barriers and Kinetic and Equilibrium Isotope Effects from Density-Functional Theory[†]Yun Liu,[‡] Brent A. Gregersen,[‡] Alvan Hengge,[§] and Darrin M. York^{*,‡}*Department of Chemistry, University of Minnesota, 207 Pleasant Street SE, Minneapolis, Minnesota 55455-0431, and Department of Chemistry and Biochemistry, Utah State University, Logan, Utah 84322-0300**Received May 2, 2006*

ABSTRACT: Primary and secondary kinetic and equilibrium isotope effects are calculated with density-functional methods for the in-line dianionic methanolysis of the native (unsubstituted) and thio-substituted cyclic phosphates. These reactions represent reverse reaction models for RNA transesterification under alkaline conditions. The effect of solvent is treated with explicit (single and double) water molecules and self-consistently with an implicit (continuum) solvation model. Singly substituted reactions at the nonbridging O_{P1} position and bridging O_{2'}, O_{3'}, and O_{5'} positions and a doubly substituted reaction at the O_{P1} and O_{P2} positions were considered. Aqueous free energy barriers are calculated, and the structures and bond orders of the rate-controlling transition states are characterized. The results are consistent with available experimental data and provide useful information for the interpretation of measured isotope and thio effects used to probe mechanism in phosphoryl transfer reactions catalyzed by enzymes and ribozymes.

The most prominent mechanism for cell signaling, energy conversion, and the synthesis and breakdown of nucleic acids involves the transfer of phosphoryl groups. Consequently, phosphoryl transfer reactions have been the focus of considerable research effort with both experimental and theoretical methods (1–4). The characterization of nonenzymatic mechanisms of phosphoryl transfer is the first step in understanding the key factors that influence reactivity and regulation of the biologically catalyzed reactions. Toward this end, a synergy between experiment and theory may offer potentially the deepest new insights into these problems.

A common experimental strategy for probing mechanism is to introduce site-specific chemical modifications into the native system and study the effect of these modifications on the reaction pathway and rate. Typically, these modifications should be sufficiently subtle that the reaction mechanism is only perturbed, and the resulting experimental data provide information that can be used to make inferences about mechanism. In the case of phosphoryl transfer reactions, two of the most common chemical modifications involve isotope (4, 5) and thio (3, 6) substitutions at the key phosphoryl oxygen positions. A change in the reaction rate constant or equilibrium constant that results from isotope substitution is known as a kinetic or equilibrium isotope effect (KIE¹ or EIE, respectively). A change in the reaction rate constant

that results from thio substitution is termed a “thio effect”. Isotope effects are sensitive probes for specific changes in bonding in the rate-controlling transition state. Thio effects provide information about protonation state and the catalytic role of certain metal ions through the measurement of associated “rescue effects” created by replacement of native hard ions, such as Mg(II) in the case of the hammerhead ribozyme (7, 8), with a more thiophilic ion such as Mn(II) or Cd(II). Measurements of isotope and thio effects have been used to study both enzymatic and nonenzymatic phosphoryl transfer reactions (1–4, 9) and, taken together, provide twofold insight into the nature of the transition states and reaction mechanisms. The interpretation of the experimental data, however, may not always be made unambiguously as multiple mechanistic pathways are often able to fit the observed kinetics equally well (10).

Computational quantum models (11–14) provide a useful tool in the elucidation of important details of biological phosphoryl transfer reactions (15–31) and may assist in the mechanistic interpretation of experimental data (10, 32). Relatively few electronic structure studies, however, have addressed the issue of the effect of sulfur substitution on biological phosphate systems (33–38). Experimental data are crucial in validating existing theoretical methods and influence the design of new-generation models, and it is important for the continued development of improved models to provide benchmark comparisons with the experimental approaches.

Of particular interest in this work is the study of a model reaction for the cleavage transesterification reaction (Scheme 1) that occurs in RNA and is catalyzed by the prototype RNA

[†] This work was supported by the National Institutes of Health (Grant GM62248 to D.M.Y. and Grant GM47297 to A.H.) and by the Army High Performance Computing Research Center (AHPCRC, to D.M.Y.) under the auspices of the Department of the Army, Army Research Laboratory (ARL) under Cooperative Agreement DAAD19-01-2-0014. Computational resources were provided by the Minnesota Supercomputing Institute.

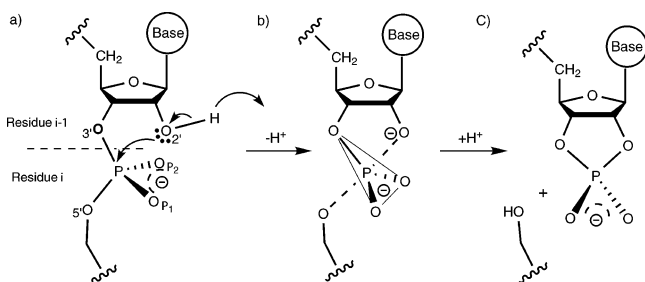
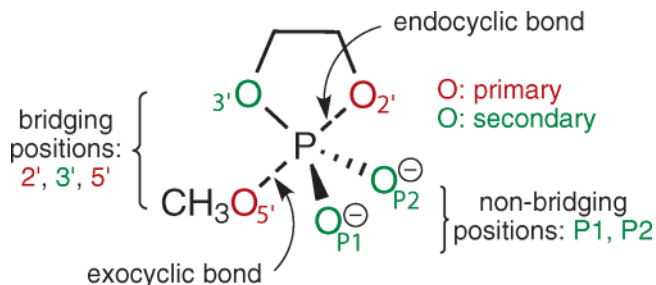
* To whom correspondence should be addressed. Phone: (612) 624-8042. Fax: (612) 626-7541. E-mail: york@chem.umn.edu.

[‡] University of Minnesota.

[§] Utah State University.

¹ Abbreviations: DFT, density-functional theory; EIE, equilibrium isotope effect; KIE, kinetic isotope effect; NBO, natural bond order; PCM, polarizable continuum model; QM/MM, quantum mechanical/molecular mechanical.

Scheme 1: RNA Transesterification

Scheme 2: Phosphorane Transition State Showing Phosphoryl Oxygen Positions for Thio Modifications and ^{18}O and ^{34}S Isotope Substitutions^a

^a An isotope effect is termed primary if a bond to the labeled atom is formed or cleaved during the reaction and secondary otherwise.

enzymes such as the hammerhead (7, 39), and hairpin (40, 41) and hepatitis delta virus (42, 43) ribozymes. Much information about the nature of the rate-controlling transition state can be gleaned from measurement of KIEs (4). The calculation of KIEs from quantum chemical models is a topic of considerable effort and importance (14, 44–51). An isotope effect is termed primary if a bond to the labeled atom is formed or cleaved during the reaction and secondary otherwise. To date, experimental KIE measurements have concentrated on acyclic phosphate monoester systems. However, advances in isotope ratio mass spectrometers may soon allow one to measure the $^{16}\text{O}:$ ^{18}O ratio for other volatile compounds bearing oxygen atoms such as the cyclic phosphate diesters (the more relevant model for ribozyme catalysis). The ring structure may, however, further complicate the mechanistic interpretation of such measurements, making theoretical work that could aid in this interpretation immediately interesting and significant.

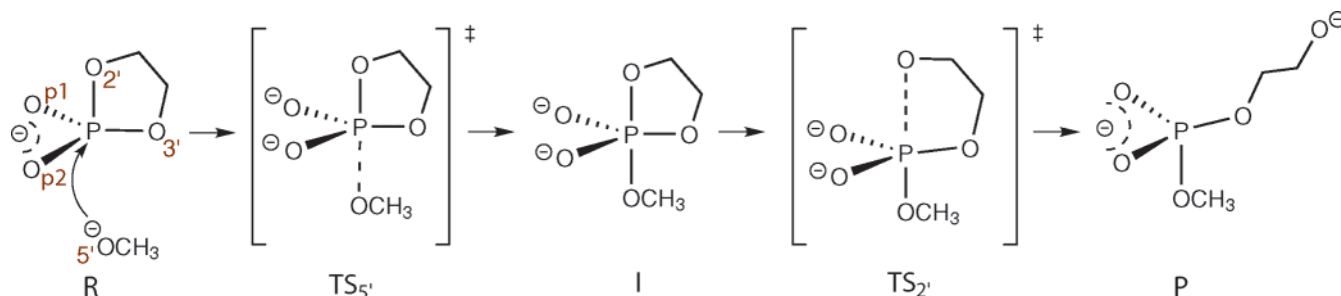
This work applies density-functional electronic structure methods to the study of primary and secondary kinetic and

equilibrium isotope effects (4, 5) on the in-line dianionic reaction mechanism for methanolysis of ethylene phosphate (Scheme 3), a reverse reaction model for RNA phosphate transesterification under alkaline conditions (1). The effect of solvent is treated with explicit (single and double) water molecules and self-consistently with an implicit (continuum) solvation model. In addition, a series of five thio substitutions (52) at the key phosphoryl oxygen positions are considered. Two primary and three secondary (^{18}O and ^{34}S) isotope effects are considered for each of the in-line dianionic reactions: the native (unsubstituted) reaction, singly substituted reactions at the nonbridging $\text{O}_{\text{P}1}$ position and bridging $\text{O}_{2'}$, $\text{O}_{3'}$, and $\text{O}_{5'}$ positions, and a doubly substituted reaction at the $\text{O}_{\text{P}1}$ and $\text{O}_{\text{P}2}$ positions (Scheme 2).

METHODS

Density-functional calculations were performed using the B3LYP exchange-correlation functional (53, 54) with the 6-31++G(d,p) basis set for geometry and frequency calculations followed by single-point energy refinement and natural bond order (NBO) analysis (55) with the 6-311++G(3df, 2p) basis set in a manner analogous to recent studies of biological phosphates (35, 56–58). Solvent was treated using the PCM solvation model (59, 60) with UAKS radii (61).

For all calculations that did not include explicit water molecules (with the exception of the “nat*” reaction; see below), solvent-relaxed geometries were optimized self-consistently with the PCM solvation model (59, 60). In the remaining calculations that considered the native reaction in the presence of zero, one, and two explicit water molecules, implicit (PCM) solvation corrections were based on gas phase-optimized geometries as in prior work (35, 56–58). Energy minimum and transition state geometry optimizations were carried out in redundant internal coordinates with default convergence criteria (62), while the stability conditions of the restricted closed shell Kohn–Sham determinant for each final structure were verified (63, 64). Frequency calculations were performed to establish the nature of all stationary points. Thermodynamic properties at 298.15 K were obtained from the density-functional calculations (unscaled frequencies) using standard statistical mechanical expressions for separable vibrational, rotational, and translational contributions within the harmonic oscillator, rigid rotor, ideal gas/particle-in-a-box models in the canonical ensemble (65) and have been described in detail elsewhere

Scheme 3: In-Line Dianionic Mechanism of Ethylene Phosphate Methanolysis (a reverse reaction model for RNA phosphate transesterification)^a

^a Although intermediate I for the native (unsubstituted) reaction is either nonexistent or only meta-stable in solution, this is not necessarily the case for certain thio substitutions. Hence, this general scheme is meant to encompass and illustrate all the possible stationary points along the reaction path for the dianionic in-line mechanism with and without thio substitutions that are discussed in this work.

(56). All electronic structure calculations were performed with the GAUSSIAN03 suite of programs (66).

The native (unsubstituted) reaction (Scheme 3) was modeled using both implicit and explicit solvation models. The first model, designated “native”, was based on solvent-relaxed geometries optimized self-consistently with the PCM in the absence of explicit waters. Three additional models based on gas phase-optimized geometries with PCM postoptimization solvation corrections were considered in the presence of zero, one, and two water molecules. The reactions are designated “nat*”, “nat:H₂O*”, and “nat:2H₂O*”, respectively, the asterisk emphasizing that PCM solvation was treated as a postoptimization correction based on the “gas phase”-optimized geometries (i.e., geometries optimized in the absence implicit PCM solvation). The remainder of the reactions were based on implicit solvent-relaxed geometries optimized self-consistently with PCM in the absence of explicit water molecules, analogous to the native reaction. A series of four single thio substitutions at the bridging O₂, O₃, and O₅ positions and nonbridging O_{P1} position, as well as a doubly substituted reaction at the O_{P1} and O_{P2} positions were considered. These reactions are designated S:O₂, S:O₃, S:O₅, S:O_{P1}, and S:O_{P1},O_{P2}, respectively. For each of these reactions, two primary and three secondary (¹⁸O and ³⁴S) kinetic and equilibrium isotope effects (Scheme 2) were calculated at 298.15 K from the conventional transition state theory (67) as implemented in POLYRATE version 9.3.1 (68). POLYRATE reads the analytical Cartesian Hessian matrix from GAUSSIAN03 [calculated at the B3LYP/6-31++G(d,p) level in this work] and, after mass weighting and projection of the six translational and rotational modes, returns the normal-mode vibrational frequencies [which satisfy the Redlich–Teller product rule (69)] and calculates the full (unscaled) vibrational and rotational partition functions within the harmonic oscillator/rigid rotor approximations. The reaction rates and isotope effects are calculated from conventional transition state theory consistent with the Bigeleisen–Mayer formalism (45, 70) and, in this work, neglect tunneling effects and changes in the transmission coefficient. A more complete treatment of kinetic isotope effects that include a fully explicit solvated environment could be made with a combined quantum mechanical/molecular mechanical (QM/MM) potential (52, 71–73) and using variational transition state theory (44, 74). This work represents an important first step in this direction.

RESULTS AND DISCUSSION

Scheme 3 illustrates the general mechanism for dianionic in-line methanolysis of ethylene phosphate with phosphoryl oxygen positions labeled in accord with their RNA counterparts involved in RNA transesterification (Scheme 1). Figure 2 illustrates the free energy profiles for in-line methanolysis of native and thio-substituted ethylene phosphate. The aqueous free energy (ΔG_{aq}) values for stationary points of the native and thio-substituted reactions are listed in Table 1. Bond lengths, bond orders, and NBO charge values for key phosphoryl oxygens in the rate-controlling transition states are listed in Table 2. Kinetic isotope effects for *p*-nitrophenyl phosphate (used as a benchmark) are listed in Table 3, and calculated KIE and EIE values for the ethylene phosphate methanolysis reaction models are listed in Table 4. To aid in the interpretation of the calculated KIE

Table 1: Relative Free Energy Values (ΔG_{aq}) for Stationary Points of Dianionic Ethylene Phosphate Methanolysis Reactions Optimized in Solution^a

reaction	TS _{X5'}	I	TS _{X2'}	P	Rev
nat*	41.1	-28.3	—	—	12.8
nat:H ₂ O*	41.1	-27.6	—	—	13.5
nat:2H ₂ O*	38.4	-24.4	—	—	14.0
native	40.4	-9.9	30.5	-0.3	30.2
S:O _{P1}	41.3	-13.0	28.3	8.6	36.9
S:O _{P1} ,O _{P2}	42.4	-16.1	26.3	11.3	37.6
S:O _{3'}	36.0	-8.9	27.1	8.1	35.2
S:O _{5'}	—	—	—	—	52.4
S:O _{2'}	38.7	-47.6	—	—	-8.9

^a Aqueous free energy values for stationary points along the reaction coordinate for in-line dianionic methanolysis for the native and thio-substituted model systems. Shown also is the reverse free energy barrier (Rev). The molecules superscripted by an asterisk “*” indicate that their structures were based on gas phase-optimized geometries and the free energies were post-corrected with PCM model. All other structures were optimized self-consistently with the PCM solvation model. Rate-controlling transition states are shown in **boldface** type, and the relative free energy values between stationary points are shown in *italics*.

Table 2: Bond Lengths, Bond Orders, and NBO Charge Values for Key Phosphoryl Oxygens (sulfurs) in the Rate-Controlling Transition State Optimized in Solution^a

Reaction	$r_{X5'}$	$r_{X2'}$	$r_{X3'}$	r_{XP1}	r_{XP2}
nat*	2.453	1.841	1.723	1.506	1.514
nat:H ₂ O*	2.572	1.792	1.702	1.510	1.518
nat:2H ₂ O*	2.431	1.865	1.688	1.511	1.514
native	2.364	1.764	1.687	1.524	1.525
S: O _{P1}	2.494	1.740	1.681	2.039	1.519
S: O _{P1} ,O _{P2}	2.619	1.732	1.683	2.028	2.022
S: O _{3'}	2.314	1.762	2.185	1.527	1.529
S: O _{5'}	2.303	2.287	1.675	1.528	1.527
S: O _{2'}	2.427	2.356	1.667	1.519	1.517
Reaction	$BO_{X5'}$	$BO_{X2'}$	$BO_{X3'}$	BO_{XP1}	BO_{XP2}
nat*	0.148	0.491	0.607	1.130	1.124
nat:H ₂ O*	0.108	0.528	0.632	1.115	1.103
nat:2H ₂ O*	0.152	0.470	0.633	1.121	1.104
native	0.170	0.531	0.625	1.085	1.089
S: O _{P1}	0.153	0.553	0.631	1.200	1.105
S: O _{P1} ,O _{P2}	0.138	0.555	0.609	1.257	1.276
S: O _{3'}	0.189	0.528	0.798	1.062	1.066
S: O _{5'}	0.647	0.216	0.638	1.059	1.076
S: O _{2'}	0.154	0.615	0.636	1.101	1.110
Reaction	$Q_{5'}$	$Q_{2'}$	$Q_{3'}$	Q_{P1}	Q_{P2}
nat*	-0.997	-0.889	-0.859	-1.210	-1.212
nat:H ₂ O*	-1.000	-0.883	-0.853	-1.209	-1.213
nat:2H ₂ O*	-0.961	-0.902	-0.850	-1.208	-1.204
native	-1.009	-0.892	-0.868	-1.238	-1.237
S: O _{P1}	-1.003	-0.889	-0.871	-0.872	-1.205
S: O _{P1} ,O _{P2}	-0.999	-0.891	-0.875	-0.793	-0.773
S: O _{3'}	-0.985	-0.896	-0.175	-1.238	-1.235
S: O _{5'}	-0.329	-0.979	-0.888	-1.234	-1.230
S: O _{2'}	-1.016	-0.348	-0.873	-1.213	-1.209

^a Shown are the P–X bond lengths (r_X) in Å, NBO⁵⁵ P–X original bond orders, and the NBO⁵⁵ charge values (Q_X) in *au*, where *X* indicates either an oxygen or sulfur atom bonded to P. The molecules with * indicate that their structures were based on gas phase-optimized geometries and the free energies were post-corrected with PCM model. The others were optimized self-consistently with the PCM solvation model.

and EIE values, Table 5 lists the bond orders from phosphorus to the primary and secondary positions in the reactant, rate-controlling transition state, and product structures for each reaction.

Table 3: Comparison of the Kinetic Isotope Effects for Reactions of *p*-Nitrophenyl Phosphate^a

model	¹⁵ <i>k</i>	¹⁸ <i>k</i> _{bridge}	¹⁸ <i>k</i> _{nonbridge}	<i>T</i> (K)
Dianionic				
experiment	1.0028	1.0189	0.9994	368
POLYRATE	1.0016	1.0137	1.0054	368
POLYRATE	1.0018	1.0162	1.0056	298
Monoanionic				
experiment	1.0005	1.0094	1.0199	308
POLYRATE	1.0020	1.0139	1.0031	308
POLYRATE	1.0020	1.0147	1.0030	298

^a A KIE value is defined as k/k' , where k and k' are the rate constants for the light and heavy isotopes, respectively. Both dianionic and monoanionic models that represent the reaction in solution under alkaline and acidic conditions, respectively, were considered. Both the dianionic and monoanionic *p*-nitrophenyl phosphate systems were optimized in the presence of one explicit water molecule.

Table 4: Primary and Secondary Kinetic (KIE) and Equilibrium (EIE) Isotope Effects for the Native and Thio-Substituted In-Line Dianionic Mechanism of Ethylene Phosphate Methanolysis^a

reaction	primary		secondary		
	X _{5'}	X _{2'}	X _{3'}	X _{P1}	X _{P2}
KIE Values (POLYRATE) in Solution					
nat*	1.0216	1.0056	1.0025	0.9962	0.9979
nat:H ₂ O*	1.0230	1.0060	1.0046	1.0016	1.0042
nat:2H ₂ O*	1.0154	1.0122	1.0005	1.0039	0.9994
native	1.0175	1.0070	1.0014	1.0011	1.0036
S:O _{P1}	1.0230	1.0046	1.0015	1.0022	1.0051
S:O _{P1} ,O _{P2}	1.0214	1.0035	1.0013	1.0002	1.0003
S:O _{3'}	1.0142	1.0066	1.0019	1.0064	1.0081
S:O _{5'}	0.9936	1.0549	1.0045	1.0043	1.0041
S:O _{2'}	1.0147	1.0056	1.0000	0.9997	1.0025
EIE Values (POLYRATE) in Solution					
nat*	0.9636	1.0327	0.9965	0.9951	0.9958
nat:H ₂ O*	0.9612	1.0392	0.9980	1.0001	1.0023
nat:2H ₂ O*	0.9608	1.0356	1.0023	1.0003	0.9986
native	0.9587	1.0361	1.0073	1.0047	1.0028
S:O _{P1}	0.9592	1.0302	1.0077	1.0052	1.0063
S:O _{P1} ,O _{P2}	0.9595	1.0261	1.0055	0.9956	0.9954
S:O _{3'}	0.9615	1.0314	1.0057	1.0126	1.0077
S:O _{5'}	0.9916	1.0316	1.0085	0.9980	1.0001
S:O _{2'}	0.9582	1.0126	1.0077	0.9934	1.0016

^a A KIE value is defined as k/k' , where k and k' are the rate constants for the light and heavy isotopes, respectively. EIE values are similarly defined using the corresponding equilibrium constants. Isotope substitutions include ¹⁸O for oxygen and ³⁴S for sulfur and are calculated at 298.15 K within the quantum harmonic oscillator approximation, neglecting changes in the transmission coefficient. Asterisks indicate that these structures were based on gas phase-optimized geometries and the free energies were postcorrected with the PCM model. The others were optimized self-consistently with the PCM solvation model.

Mechanism and Free Energy Barriers for the Native Reaction

The native reaction models with zero, one, or two explicit water molecules optimized in the absence of implicit solvation (nat*, nat:H₂O*, and nat:2H₂O*, respectively) all proceed through a single early transition state, TS_{5'} (Figure 1), with an elongated P–O_{5'} bond (2.453, 2.572, and 2.431 Å, respectively) and considerably distorted trigonal bipyramidal structure ($\theta_{ax} = 163.2, 162.3,$ and 163.3° , respectively) and result in an acyclic phosphodiester with the 2'-alkoxide leaving group extended to 5 Å from the phosphorus and forming a right angle ($\sim 90^\circ$) with the 5'-nucleophile. The –O–CH₂–CH₂–O_{2'}[–] chain of the product structure is in a trans conformation around the C–C single bond.

Table 5: Comparison of Bond Orders in the Reactants, Rate-Controlling Transition States, and Products of Dianionic Ethylene Phosphate Methanolysis Reactions Optimized in Solution^a

state	BO _{X_{5'}}	BO _{X_{2'}}	BO _{X_{3'}}	BO _{X_{P1}}	BO _{X_{P2}}
nat* Reaction					
reactant	–	0.608	0.608	1.161	1.161
TS	0.148	0.491	0.607	1.130	1.124
product	0.606	–	0.662	1.129	1.117
nat:H ₂ O* Reaction					
reactant	–	0.624	0.624	1.137	1.137
TS	0.108	0.528	0.632	1.115	1.103
product	0.624	0.003	0.682	1.105	1.090
nat:2H ₂ O* Reaction					
reactant	–	0.628	0.639	1.154	1.088
TS	0.152	0.470	0.633	1.121	1.104
product	0.622	0.003	0.685	1.096	1.081
native Reaction					
reactant	–	0.633	0.633	1.136	1.136
TS	0.170	0.531	0.625	1.085	1.089
product	0.636	–	0.659	1.110	1.108
S:O _{P1} Reaction					
reactant	–	0.635	0.631	1.298	1.140
TS	0.153	0.553	0.631	1.200	1.105
product	0.630	–	0.675	1.258	1.112
S:O _{P1} ,O _{P2} Reaction					
reactant	–	0.615	0.615	1.340	1.340
TS	0.138	0.555	0.609	1.257	1.276
product	0.615	–	0.661	1.302	1.293
S:O _{3'} Reaction					
reactant	–	0.630	0.795	1.124	1.125
TS	0.189	0.528	0.798	1.062	1.066
product	0.631	–	0.845	1.105	1.095
S:O _{5'} Reaction					
reactant	–	0.633	0.633	1.136	1.136
TS	0.647	0.216	0.638	1.059	1.076
product	0.812	–	0.652	1.094	1.109
S:O _{2'} Reaction					
reactant	–	0.795	0.630	1.125	1.124
TS	0.154	0.615	0.636	1.101	1.110
product	0.637	–	0.656	1.107	1.114

^a Shown are the NBO (55) P–X original bond orders. Asterisks indicate that these structures were based on gas phase-optimized geometries and the free energies were postcorrected with the PCM model. The others were optimized self-consistently with the PCM solvation model.

A notable feature of the native reaction optimized self-consistently with the PCM solvation model is the appearance of a shallow metastable phosphorane intermediate with a negligible barrier to the late TS_{2'} transition state (which is not rate-limiting) and collapse to the product state. The very small, negative “barrier” (–0.3 kcal/mol) reported in Table 1 to the TS_{2'} transition state arises from the fact that the geometries were optimized with a 6-31++G(d,p) basis set and then the energy values were refined with a 6-311++G-(3df,2p) basis set. In this case, kinetically insignificant intermediate “I” for the native reaction at the B3LYP/6-31++G(d,p) level optimized with PCM disappears (ceases to be a stationary point) at the B3LYP/6-311++G(3df,2p) level. Intermediate I and TS_{2'} are slightly more in-line in terms of the θ_{ax} angles (167.8 and 168.6°) than TS_{5'} (166.5°). The calculated results suggest the rate-controlling transition state corresponds to the formation of the P–O_{5'} bond.

Inclusion of implicit solvation in the geometry optimization procedure leads to a more associative rate-controlling TS_{5'} transition state, as indicated by the native reaction model

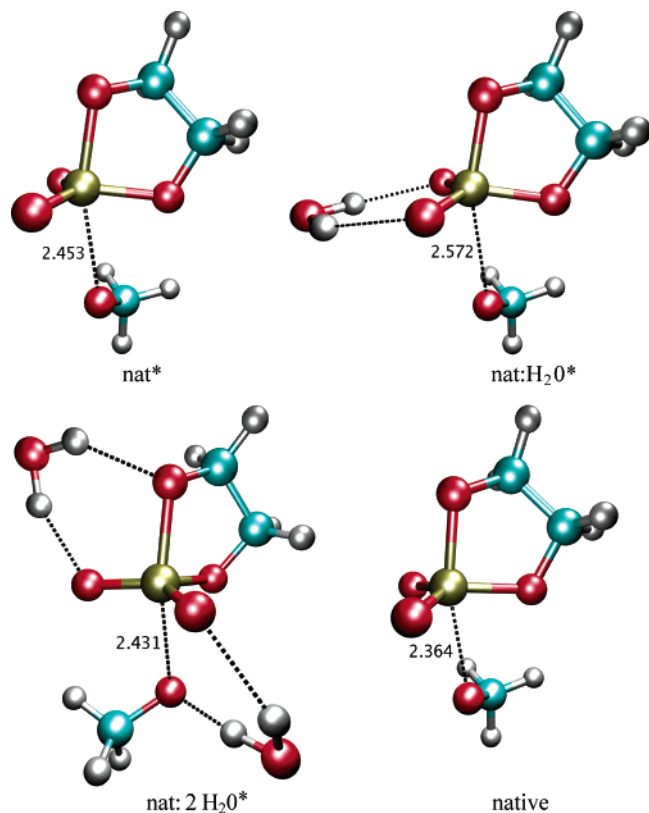


FIGURE 1: Rate-controlling transition state structures for in-line methanolysis of ethylene phosphate based on reaction models with different implicit and explicit solvation.

having the shortest P–O_{5'} bond (2.364 Å). This arises from the effect of solvent in screening Coulomb repulsions and favoring a more compact cavity for the dianionic transition state. The models without implicit solvent relaxation are less associative and have slightly greater metaphosphate character as measured by the sum of the bond orders to the nucleophilic and leaving group positions. This is particularly so in the nat:2H₂O* model where a water molecule bridging the O_{P2} and O_{2'} positions stabilizes the accumulating charge at the O_{2'} leaving group, causing the bond length to increase to 1.865 Å and the bond order to decrease to 0.470 (Table 2).

The forward and reverse native reaction barriers (Table 1) are similar for the native reaction models optimized with explicit and implicit water. The forward barriers span a 2.7 kcal/mol range from 38.4 kcal/mol (nat:2H₂O*) to 41.1 kcal/mol (nat* and nat:H₂O*), and reverse barriers span a 4.4 kcal/mol range from 24.4 kcal/mol (nat:2H₂O*) to 28.8 kcal/mol (native). It is notable that the barriers in the presence of two explicit waters (nat:2H₂O*) are the lowest, suggesting that specific hydrogen bonds are important for transition state stabilization. The absolute values of the barriers, however, are likely considerably too high on the basis of estimated rates of hydrolysis of dimethyl phosphate and the relative rates of hydrolysis of dimethyl and ethylene phosphate (21). The main sources of the probable elevated rates calculated with the PCM model employed here are likely the lack of explicit hydrogen bonding, proper treatment of charge penetration and dielectric saturation, and the neglect of appropriate changes in cavity size with charge state. In principle, simulations with hybrid QM/MM models with explicit solvent offer a more robust method for calculating mechanisms and barriers for these types of reactions;

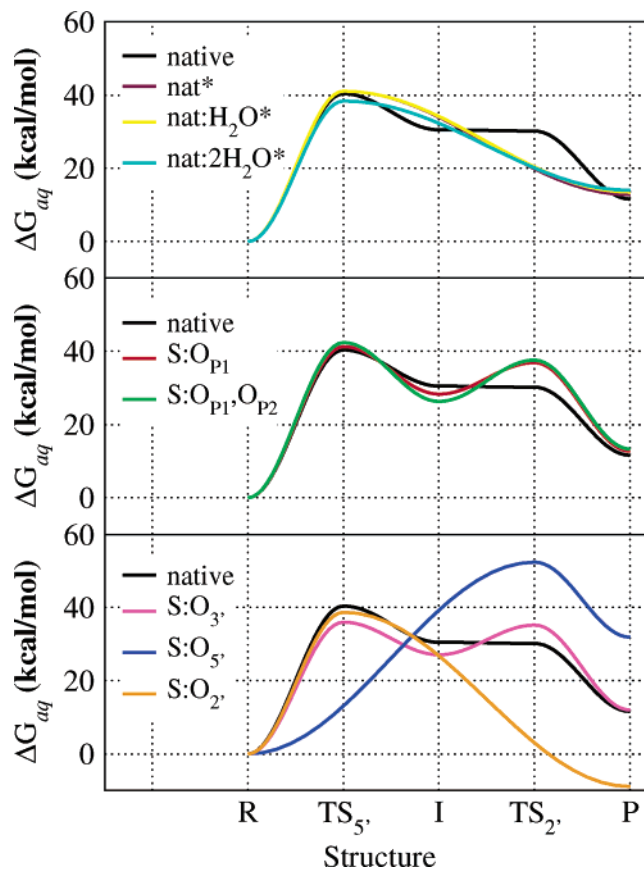


FIGURE 2: Free energy profiles for dianionic native and thio-substituted ethylene phosphate methanolysis reactions optimized self-consistently with the PCM solvation model (plots have been smoothed for clarity; only stationary points designated on the horizontal axis were computed).

however, a necessary first step in this direction is to develop accurate quantum methods that, unlike the costly density-functional models applied here, are sufficiently fast to be applied in QM/MM simulations. The quantum results presented herein, therefore, may also aid in the design of new semiempirical quantum models for phosphoryl transfer reactions and RNA catalysis.

Thio Effects at the Bridging and Nonbridging Phosphoryl Positions

Substitutions at the Nucleophilic and Leaving Group Positions (5'/2'). Sulfur substitution at the nucleophilic 5' position (S:O_{5'}) for the methanolysis reactions in solution (i.e., changing the methoxide nucleophile to methanethiolate) has a dramatic effect on the mechanism and leads to a single TS_{2'} transition state with an almost fully formed P–S_{5'} bond (2.303 Å) that is only 0.142 Å longer than that of the product structure and an elongated P–O_{2'} bond (2.287 Å). The shift of the rate-controlling transition state to that of a TS_{2'} type is accompanied by a large increase in the free energy of activation (52.4 kcal/mol) and reaction free energy (31.9 kcal/mol) relative to those of the native reaction. This is largely due to the increased stability of the thiolate nucleophile in solution [methanethiol has a pK_a value 5 units lower than that of methanol (75)] that leads to a dramatic decrease in the reverse activation barrier of 8.3 kcal/mol. This is qualitatively consistent with the experimentally observed transesterification of 5'-phosphorothioates (76, 77) that is

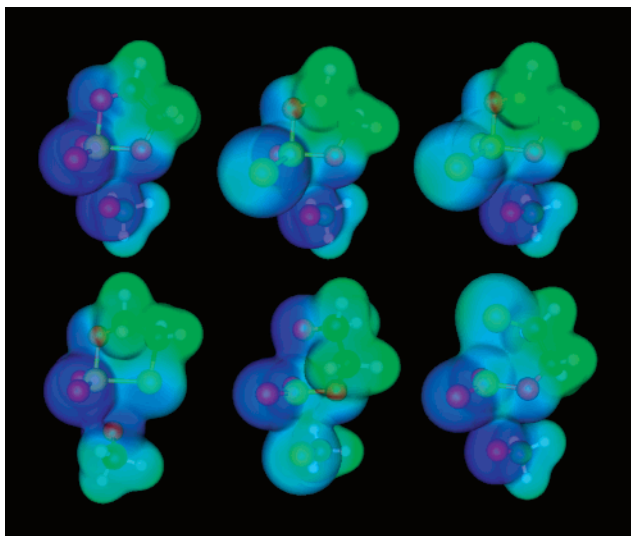


FIGURE 3: Electrostatic potential mapped onto the molecular van der Waals surface for rate-controlling transition state structures in the gas phase for dianionic native and thio-substituted reactions: (top) native, S:O_{P1}, and S:O_{P1},O_{P2} from left to right and (bottom) S:O_{3'}, S:O_{5'}, and S:O_{2'} from left to right.

4–5 orders of magnitude faster than the corresponding native reaction at alkaline pH.

As opposed to that of the S:O_{5'} reaction, sulfur substitution at the leaving group 2' position (S:O_{2'}) results in a single early TS_{5'} transition state with an elongated P–O_{5'} bond (2.427 Å). The S:O_{2'} reaction has a forward activation barrier that is 1.7 kcal/mol lower and a reaction free energy that is 20.5 kcal/mol lower than those of the native reaction. The dramatically decreased reaction free energy increases the reverse transesterification activation barrier by 18.8 kcal/mol. In these cases, the reaction rate of transesterification is considerably slower than that of the native reaction at alkaline pH. Therefore, transesterification of 2'-thio-substituted phosphates has been observed only in the presence of strongly electronegative leaving groups (3). As reported by Dantzman et al. (78), the rate of the attack of the thiolate on the adjacent phosphodiester bond is 10⁷-fold slower than that of the corresponding alkoxide for the transesterification reaction of 2'-deoxy-2'-thiouridine 3'-(*p*-nitrophenyl phosphate), corresponding to a roughly 10 kcal/mol difference in free energy. The large increase in the barrier (18.8 kcal/mol) for the dianionic reaction upon 2' thio substitution is in qualitative agreement with this experimental observation.

Substitution at the 3' Position. Sulfur substitution at the 3' position (S:O_{3'}) has some minor effects on the mechanism. TS_{5'} exhibits slightly more associative character with a P–O_{5'} bond length of 2.314 Å. The 3'-sulfur in the equatorial position strengthens the effective repulsions with the axial ligands around phosphorus and leads to a distortion of the trigonal bipyramidal structure of TS_{5'} ($\theta_{ax} = 162.9^\circ$) by 3.6° relative to the native reaction.

Substitution at the bridging O_{3'} position leads to a decrease in the activation barrier of 4.4 and 4.8 kcal/mol for the forward methanolysis and reverse transesterification reactions, respectively. Sulfur substitution at the 3' position has a stabilizing electronic effect in the dianionic transition state and weakens the effective repulsions in the exocyclic bond formation step. Also, 3' substitution can lead to geometric changes in the backbone due to the elongated bonds and

sharpened angles. Hence, the relief of the strain energy in the five-membered ring (2, 79, 80) also stabilizes the cyclic transition state.

Due to the origin of the moderate reaction rate acceleration that is produced, the effects of sulfur substitution at the 3' position have been the focus of several experimental studies (2, 3). It is observed that the base-catalyzed cleavage of the thio-modified RNA is 200–2000-fold faster than the native reaction (80), corresponding to an aqueous free energy barrier relaxation of 3–4.5 kcal/mol. The calculated barrier relaxation of 4.8 kcal/mol for S:O_{3'} transesterification is in reasonable agreement with this estimated experimental result.

Substitution at the Nonbridging Positions (O_{P1} and O_{P2}). Sulfur substitution at the nonbridging phosphoryl oxygen positions (O_{P1} and O_{P2}) results in an earlier TS_{5'} with less associative character: the P–O_{5'} bond length increases from 2.364 Å in the native reaction to 2.494 and 2.619 Å in the singly (S:O_{P1}) and doubly (S:O_{P1},O_{P2}) substituted reactions, respectively. TS_{5'} becomes a later transition state with longer P–O_{2'} bonds with an increased level of sulfur substitution at the nonbridging positions, analogous to the lengthening of the P–O_{5'} bonds with an increased level of sulfur substitution in TS_{5'}.

Single and double sulfur substitution at the nonbridging positions have both electronic and solvation effects on the reaction. Since the nonbridging O_{P1} and O_{P2} positions carry the majority of the negative charge and increase in anionic character when one moves from the reactant to the transition state, the softer, more polarizable sulfur in the nonbridging position can facilitate redistribution of the charge and stabilization of the dianionic transition state. However, the sulfur atoms are larger and less well solvated, and thio substitution tends to produce less pronounced solvent-induced lowering of the reaction barriers. Hence, the electronic and solvation effects that occur upon sulfur substitution have the tendency to cancel one another, and the single and double sulfur substitution at the nonbridging positions thus have only a small effect on the activation barrier and the reaction free energy compared with the native reaction. In the case of the forward methanolysis reaction, barrier increases of 0.9 and 2.0 kcal/mol are observed for single (S:O_{P1}) and double (S:O_{P1},O_{P2}) thio substitutions, respectively. In the case of the reverse transesterification reaction, the barrier changes are less pronounced with values of –0.2 and 0.3 kcal/mol for single and double thio substitutions, respectively.

Experimental studies of thio effects at the nonbridging phosphoryl oxygen positions provide a useful mechanistic probe into enzymatic and nonenzymatic RNA hydrolysis and the role of metal binding. Single thio substitution at the nonbridging positions shows almost no effect on the alkaline cleavage rate for various dinucleotides (6, 81–86). Oivanen et al. (87) found a negligible kinetic thio effect for the alkaline hydrolysis of 3',5'-UpU. Almer et al. (82, 83) reported rate constant $k(\text{phosphate})/k(\text{thiophosphate})$ ratios of 1.3 and 0.78 at the R_p and S_p positions, respectively, for 3',5'-Up(s)U. The calculated moderate thio effects for the alkaline transesterification (–0.2 kcal/mol) and methanolysis (0.9 kcal/mol) for the S:O_{P1} reaction strongly agree with the experimental results described above. Compared with that of single thio substitution, the effect of double thio substitution at the nonbridging positions is more controversial. Nielsen et al. (88, 89) observed a higher chemical and

enzymatic stability for the phosphorodithioate linkage in RNA than in natural RNA. However, more recently, Ora et al. (86) have determined that replacement of the remaining nonbridging oxygen of phosphoromonothioates with sulfur has a surprisingly small effect on the kinetics of hydrolysis and transesterification at alkaline pH. These calculations on dianionic S:O_{P1},O_{P2} show very moderate elevation of the methanolysis and transesterification aqueous free energy barriers (2.0 and 0.3 kcal/mol, respectively) and support the latter experimental data.

Primary and Secondary Equilibrium and Kinetic Isotope Effects

Testing and Validation of KIE Values for p-Nitrophenyl Phosphate. Before we examine the KIE and EIE values of the transesterification models for which there are currently no available experimental values, it is important to provide a general assessment of the overall reliability of the density-functional method to a related system in which the experimental KIE has been established. Table 3 summarizes the experimental (4) and calculated KIE values for the dissociative reaction path of both dianionic and monoanionic *p*-nitrophenyl phosphate at 368 and 308 K, respectively. The models that represent the reaction in solution under alkaline (dianionic) and acidic (monoanionic) conditions were considered, respectively. Both the dianionic and monoanionic *p*-nitrophenyl phosphate systems were optimized in the presence of one explicit water molecule at the B3LYP/6-31++G(d,p) level as described in Methods. The calculated KIE values were obtained from POLYRATE (68). For the dianionic system at the experimental temperature, the KIE values correlate reasonably with the experimental values (1.0016 compared with 1.0028 for ¹⁵*k* and 1.0137 compared with 1.0189 for ¹⁸*k*_{bridge}) with the exception that a normal KIE for ¹⁸*k*_{nonbridge} (1.0054) is calculated in contrast to the slight inverse experimental KIE (0.9994) (4). The difference is likely due to the two hydrogen bonds between the explicit water and the two nonbridging oxygens in the optimized dianionic system. For the monoanionic reaction, the calculated results are also in reasonable agreement with the experimental values (see Table 3). Overall, the qualitative agreement with the calculated and experimental KIEs for *p*-nitrophenyl phosphate is encouraging but not impressive. These results underscore the need to determine more thoroughly the sources of error in the calculated KIEs in solution that will enable the design of improved models with increased accuracy and predictive capability.

Predicted KIE Values for Transphosphorylation Reaction Models. Table 4 lists the KIE and EIE values for native and thio-substituted in-line dianionic methanolysis reactions. Table 5 compares the bond orders for the reactants, rate-controlling transition states, and products for each reaction and allows facile comparison to the changes in bond order that correlate strongly with the isotope effects shown in Table 4.

With the exception of the 5' thio substitution (S:O_{5'}), the primary KIEs are most prominent at the 5' position for all the reactions. The experimental KIE values are available for the cyclization of uridine 3'-*m*-nitrobenzyl phosphate at different pH values (90), the reverse reaction of which is similar to that of this work. A normal primary KIE (1.027)

under basic conditions (pH 10.5) was interpreted to be consistent with a concerted mechanism with the departure of an almost fully charged leaving group (90). Cassano et al. also reported the nucleophile KIE of 1.027 for the attack of hydroxide on thymidine 5'-*p*-nitrophenyl phosphate (91). The calculated primary KIE values at the 5' position for the native reaction models range from 1.0154 to 1.0230, in reasonable agreement with the KIE measurements for the related systems. Taken together with the data in Table 2 for the rate-limiting transition states of the native reaction models, including the range of P–O_{5'} bond lengths (from 2.364 to 2.572 Å), bond orders (from 0.108 to 0.170), and NBO charges of the 5'-oxygen (from –0.961 to –1.009 *e*), these data are consistent with the experimental results and interpretation (91).

The primary KIE values at the 5' position (nucleophile KIEs) arise from two contrasting contributions: (1) P–O bond formation, which is always inverse, and (2) the imaginary frequency factor (sometimes termed reaction coordinate motion) which, since the imaginary frequency is larger for the lighter isotope, is always normal (91–93). Early transition states give rise to the largest normal nucleophile KIEs, since the imaginary frequency factor is dominant, as in the transition states for all the reactions with the exception of the 5' thio substitution. As transition states become later with more bond formation, the nucleophile KIE becomes smaller and finally inverse, as in the S:O_{5'} transition state.

KIE Values for Native Reaction Models. In the four native reaction models (nat*, nat:H₂O*, nat:2H₂O*, and native), the reaction optimized in the presence of two explicit water molecules (nat:2H₂O*) has the smallest primary X_{5'} KIE (1.0154) but an elevated X_{2'} KIE (1.0122). The large X_{2'} KIE value suggests that the nat:2H₂O* reaction has a looser rate-limiting transition state with relatively extensive bond fission to leaving group (4). As shown in Tables 2 and 5, the nat:2H₂O* reaction has the smallest sum of bond orders to the nucleophilic and leaving group positions (0.622) and the water molecule bridging the O_{P2} and O_{2'} positions can stabilize the accumulating charge at the O_{2'} leaving group, causing the P–O_{2'} bond length to increase to 1.865 Å and the bond order to decrease to 0.470. The inverse KIE at the X_{P2} position also suggests that the transition state has increased metaphosphate-like character.

It is noteworthy that the inverse nonbridging KIEs (X_{P1} and X_{P2}) in the native reaction optimized in the absence of implicit solvation (nat*) change to normal in the presence of implicit solvation (native). As discussed in Mechanism and Free Energy Barriers for the Native Reaction, due to the solvent screening of the Coulomb repulsions, the dianionic transition state optimized self-consistently with solvation (native) favors a more compact cavity and gives rise to a more associative transition state. The transition state without implicit solvent relaxation (nat*) shows less associative and greater metaphosphate character as measured by the sum of the bond orders to the nucleophile and leaving group (0.639 for nat* and 0.701 for native).

KIE Values for Thio-Substituted Reaction Models. The primary X_{5'} KIE for the native reaction, 1.0175, increases to 1.0230 upon sulfur substitution of one of the nonbridging positions. This is intriguing in that a similar change was observed between the hydrolysis of the *p*-nitrophenyl phosphate dianion and *p*-nitrophenyl phosphorothioate (the

primary bridging ^{18}O KIE increases from 1.0189 to 1.0237) (94), despite the similarity of these reactions as indicated by other measurements (95, 96).

The primary $X_{5'}$ KIE for the $\text{S}:\text{O}_{3'}$ reaction (1.0142 compared with 1.0175 for the native reaction) suggests that this transition state is slightly later and more associative with respect to the nucleophile than that of the native reaction. This is consistent with the slightly contracted $\text{P}-\text{O}_{5'}$ distances in the rate-controlling transition state (Table 2). The $\text{S}:\text{O}_{5'}$ reaction exhibits a prominent normal primary KIE at the $2'$ position for ^{18}O substitution (1.0549) and an inverse KIE (0.9936) for ^{34}S substitution at the $5'$ position. The rate-controlling transition state for this reaction is shifted to that of a late $\text{TS}_{2'}$ with significant accumulated $\text{P}-\text{S}_{5'}$ bonding (bond order of 0.647) and increased associative character with respect to the nucleophile.

Most of the reactions show normal (>1) secondary KIE values at the $X_{3'}$, $X_{\text{P}1}$, and $X_{\text{P}2}$ positions. This suggests that the transition states have phosphorane-like character (4). Another measure of the degree of phosphorane versus metaphosphate character of a transition state involves the sum of the bond orders of the phosphorus bonds to the nucleophilic and leaving group positions. On the basis of this index, the data in Table 5 would suggest that the transition states for the native reactions with one and two explicit waters have the most metaphosphate-like character, and the transition states for the $\text{S}:\text{O}_{5'}$ and $\text{S}:\text{O}_{2'}$ reactions have the most phosphorane-like character. Examination of the bond orders suggests the $\text{S}:\text{O}_{5'}$ and $\text{S}:\text{O}_{2'}$ transition states would be better described as tetraphosphate with a very weakly formed $\text{P}-\text{S}$ bond. It should be pointed out that the numerical values of the bond orders in Tables 2 and 5 are somewhat subjective, especially when different types of bonds are being compared.

EIE Values for Native and Thio-Substituted Reaction Models. The primary EIEs are all inverse at the $5'$ position and normal at the $2'$ position. This is as expected. EIEs should always be inverse at the nucleophilic position because there is no imaginary frequency factor, and the formation of the additional bond will always favor the heavier isotope. The situation is reversed when these isotopes occupy the $2'$ position and indicates a preference for the heavier isotope to occupy a tighter bonding arrangement. The $5'$ ^{18}O or ^{34}S isotopes proceed from a more stiff bond with carbon in the reactant alkoxide/thiolate to a more loose bonding arrangement in the phosphate/phosphorothioate product. The secondary EIEs are overall considerably variable. This is somewhat in contrast to the previous EIE results based on gas phase-optimized geometries (and frequencies) and calculated within GAUSSIAN03 (66) that indicate, with the exception of the native and $\text{S}:\text{O}_{5'}$ reaction, a slight loosening occurs when the product state is reached in the gas phase (36). This is likely a result of a loosening of the nucleophilic $\text{C}_{5'}-\text{O}_{5'}$ bond that becomes elongated upon solvation (see Table 5).

Although measurements of isotope effects provide valuable information about mechanism, they do not always decisively distinguish between associative and dissociative pathways (10, 32). Consequently, the continued evaluation and improvement of theoretical methods for the prediction of isotope effects that may aid in the interpretation of experiments are important and, taken together with experimental data, provide deeper insight into the mechanism of biological phosphoryl transfer processes.

CONCLUSION

This work presents results of density-functional study of thio effects and isotope effects on the in-line mechanism of methanolysis of ethylene phosphate, a reverse reaction model for RNA transesterification. The effect of solvent is treated with explicit (single and double) water molecules and self-consistently with an implicit (continuum) solvation model. Singly substituted reactions at the nonbridging $\text{O}_{\text{P}1}$ position and bridging $\text{O}_{2'}$, $\text{O}_{3'}$, and $\text{O}_{5'}$ positions and a doubly substituted reaction at the $\text{O}_{\text{P}1}$ and $\text{O}_{\text{P}2}$ positions were considered. Aqueous free energy barriers are calculated, and the structures and bond orders of the rate-controlling transition states are characterized.

The results of this work help to connect mechanism with kinetic isotope effects for a series of reactions of cyclic phosphates. To date, the study of isotope effects has focused on acyclic phosphate monoester systems. However, advances in isotope ratio mass spectrometers may soon afford the measurement of ^{16}O and ^{18}O isotope effects for other volatile compounds bearing oxygen atoms such as the cyclic phosphate diesters (the more relevant model for ribozyme catalysis). The ring structure may, however, further complicate the mechanistic interpretation of such measurements, making the theoretical work that could aid in this interpretation considerably important.

Modeling these highly charged reactions in the complex solution, enzyme, and ribozyme environments remains a challenging task for computational quantum chemistry. Hence, it is important to provide benchmark calculations and critical assessment of existing theoretical methods, including comparison with experiment where possible, to determine the limits of reliability, and to identify directions for future model improvement. The results provided here are generally consistent with available experimental data and provide insight into the nature of isotope effects and thio effects in phosphoryl transfer reactions that are important for the mechanistic characterization of enzymes and ribozymes. However, the fact that the aqueous free energy barriers of ethylene phosphate methanolysis are considerably too high relative to experiment and the reasonable, but not perfect, agreement of kinetic and equilibrium isotope effects compared with experiments for an acyclic system show some limitations of the theoretical methods employed here. The main sources of the error in this work are likely due to the lack of explicit hydrogen bonding, the proper treatment of charge penetration and dielectric saturation, and the neglect of appropriate changes in cavity size with charge state. Areas identified as being most in need of improvement include a more sophisticated treatment of explicit solvent combined with extensive conformational sampling with, for example, accurate hybrid QM/MM methods. We are hopeful that further interplay between theory and experiment may lead to the design of new-generation quantum methods capable of modeling phosphoryl transfer reactions with improved accuracy and reliability.

REFERENCES

1. Perreault, D. M., and Anslyn, E. V. (1997) Unifying the Current Data on the Mechanism of Cleavage-Transesterification of RNA, *Angew. Chem., Int. Ed.* 36, 432–450.
2. Zhou, D.-M., and Taira, K. (1998) The Hydrolysis of RNA: From Theoretical Calculations to the Hammerhead Ribozyme-Mediated Cleavage of RNA, *Chem. Rev.* 98, 991–1026.

- Oivanen, M., Kuusela, S., and Lönnberg, H. (1998) Kinetics and Mechanisms for the Cleavage and Isomerization of the Phosphodiester Bonds of RNA by Bronsted Acids and Bases, *Chem. Rev.* 98, 961–990.
- Hengge, A. C. (2002) Isotope effects in the study of phosphoryl and sulfuryl transfer reactions, *Acc. Chem. Res.* 35, 105–112.
- Hengge, A. C. (2001) Isotope effects in the study of enzymatic phosphoryl transfer reactions, *FEBS Lett.* 501, 99–102.
- Herschlag, D., Piccirilli, J. A., and Cech, T. R. (1991) Ribozyme-Catalyzed and Nonenzymatic Reactions of Phosphate Diesters: Rate Effects upon Substitution of Sulfur for a Nonbridging Phosphoryl Oxygen Atom, *Biochemistry* 30, 4844–4854.
- Scott, W. G. (1999) Biophysical and biochemical investigations of RNA catalysis in the hammerhead ribozyme, *Q. Rev. Biophys.* 32, 241–294.
- Suzumura, K., Takagi, Y., Orita, M., and Taira, K. (2004) NMR-Based Reappraisal of the Coordination of a Metal Ion at the Pro-Rp Oxygen of the A9/G10.1 Site in a Hammerhead Ribozyme, *J. Am. Chem. Soc.* 126 (47), 15504–15511.
- Onyido, I., Swierczek, K., Purcell, J., and Hengge, A. C. (2005) A Concerted Mechanism for the Transfer of the Thiophosphinoyl Group from Aryl Dimethylphosphinothioate Esters to Oxyanionic Nucleophiles in Aqueous Solution, *J. Am. Chem. Soc.* 127, 7703–7711.
- Åqvist, J., Kolmodin, K., Florian, J., and Warshel, A. (1999) Mechanistic alternatives in phosphate monoester hydrolysis: What conclusions can be drawn from available experimental data? *Chem. Biol.* 6 (3), R71–R80.
- Karplus, M. (2000) Aspects of Protein Reaction Dynamics: Deviations from Simple Behavior, *J. Phys. Chem. B* 104, 11–27.
- Friesner, R. A., and Beachy, M. D. (1998) Quantum mechanical calculations on biological systems, *Curr. Opin. Struct. Biol.* 8, 257–262.
- Warshel, A. (2003) Computer simulations of enzyme catalysis: Methods, progress, and insights, *Annu. Rev. Biophys. Biomol. Struct.* 32, 425–443.
- Garcia-Viloca, M., Gao, J., Karplus, M., and Truhlar, D. G. (2004) How enzymes work: Analysis by modern rate theory and computer simulations, *Science* 303, 186–195.
- Lim, C., and Karplus, M. (1990) Nonexistence of dianionic pentacoordinate intermediates in an ab initio study of the base-catalyzed hydrolysis of ethylene phosphate, *J. Am. Chem. Soc.* 112, 5872–5873.
- Uchamaru, T., Tanabe, K., Nishikawa, S., and Taira, K. (1991) Ab Initio Studies of a Marginally Stable Intermediate in the Base-Catalyzed Methanolysis of Dimethyl Phosphate and Nonexistence of the Stereoelectronically Unfavorable Transition State, *J. Am. Chem. Soc.* 113, 4351–4353.
- Lim, C., and Tole, P. (1992) Concerted Hydroxyl Ion Attack and Pseudorotation in the Base-Catalyzed Hydrolysis of Methyl Ethylene Phosphate, *J. Phys. Chem.* 96, 5217–5219.
- Mercero, J. M., Barrett, P., Lam, C. W., Fowler, J. E., Ugalde, J. M., and Pedersen, L. G. (2000) Quantum Mechanical Calculations on Phosphate Hydrolysis Reactions, *J. Comput. Chem.* 21, 43–51.
- Arantes, G. M., and Chaimovich, B. (2005) Thiolysis and Alcoholysis of Phosphate Tri- and Monoesters with Alkyl and Aryl Leaving Groups. An ab Initio Study in the Gas Phase, *J. Phys. Chem. A* 109, 5625–5635.
- Dejaegere, A., Lim, C., and Karplus, M. (1991) Dianionic Pentacoordinate Species in the Base-Catalyzed Hydrolysis of Ethylene and Dimethyl Phosphate, *J. Am. Chem. Soc.* 113, 4353–4355.
- Dejaegere, A., and Karplus, M. (1993) Hydrolysis Rate Difference between Cyclic and Acyclic Phosphate Esters: Solvation versus Strain, *J. Am. Chem. Soc.* 115 (12), 5316–5317.
- Tole, P., and Lim, C. (1993) New Insights into the Base-Catalyzed Hydrolysis of Methyl Ethylene Phosphate, *J. Phys. Chem.* 97, 6212–6219.
- Tole, P., and Lim, C. (1994) The Significance of Electrostatic Effects in Phospho-Ester Hydrolysis, *J. Am. Chem. Soc.* 116 (9), 3922–3931.
- Chang, N., and Lim, C. (1997) An ab initio study of nucleophilic attack of trimethyl phosphate: Factors influencing site reactivity, *J. Phys. Chem. A* 101, 8706–8713.
- Florián, J., and Warshel, A. (1997) A fundamental assumption about OH-attack in phosphate ester hydrolysis is not fully justified, *J. Am. Chem. Soc.* 119, 5473–5474.
- Florián, J., and Warshel, A. (1998) Phosphate ester hydrolysis in aqueous solution: Associative versus dissociative mechanisms, *J. Phys. Chem. B* 102, 719–734.
- Hu, C.-H., and Brinck, T. (1999) Theoretical Studies of the Hydrolysis of the Methyl Phosphate Anion, *J. Phys. Chem. A* 103, 5379–5386.
- Lopez, X., Dejaegere, A., and Karplus, M. (2001) Solvent Effects on the Reaction Coordinate of the Hydrolysis of Phosphates and Sulfates: Application of Hammond and Anti-Hammond Postulates to Understand Hydrolysis in Solution, *J. Am. Chem. Soc.* 123, 11755–11763.
- Lopez, X., Schaefer, M., Dejaegere, A., and Karplus, M. (2002) Theoretical evaluation of pK_a in phosphoranes: Implications for phosphate ester hydrolysis, *J. Am. Chem. Soc.* 124 (18), 5010–5018.
- Chen, X., and Zhan, C.-G. (2004) Theoretical determination of activation free energies for alkaline hydrolysis of cyclic and acyclic phosphodiester in aqueous solution, *J. Phys. Chem. A* 108, 6407–6413.
- Xu, D., Guo, H., Liu, Y., and York, D. M. (2005) Theoretical Studies of Dissociative Phosphoryl Transfer in Interconversion of Phosphoenolpyruvate to Phosphonopyruvate: Solvent Effects, Thio Effects, and Implications for Enzymatic Reactions, *J. Phys. Chem. B* 109, 13827–13834.
- Florián, J., Åqvist, J., and Warshel, A. (1998) On the reactivity of phosphate monoester dianions in aqueous solution: Brønsted linear free-energy relationships do not have a unique mechanistic interpretation, *J. Am. Chem. Soc.* 120, 11524–11525.
- Liang, C., and Allen, L. C. (1987) Sulfur Does Not Form Double Bonds in Phosphorothioate Anions, *J. Am. Chem. Soc.* 109, 6449–6453.
- Florián, J., Štrajbl, M., and Warshel, A. (1998) Conformational flexibility of phosphate, phosphonate, and phosphorothioate methyl esters in aqueous solution, *J. Am. Chem. Soc.* 120, 7959–7966.
- López, C. S., Faza, O. N., Gregersen, B. A., Lopez, X., de Lera, A. R., and York, D. M. (2004) Pseudorotation of Natural and Chemically Modified Biological Phosphoranes: Implications for RNA Catalysis, *ChemPhysChem* 5, 1045–1049.
- Liu, Y., Lopez, X., and York, D. M. (2005) Kinetic isotope effects on thio-substituted biological phosphoryl transfer reactions from density-functional theory, *Chem. Commun.* 31, 3909–3911.
- Uchamaru, T., Stec, W. J., and Taira, K. (1997) Mechanism of the Chemoselective and Stereoselective Ring Opening of Oxathiaphosphoranes: An Ab Initio Study, *J. Org. Chem.* 62, 5793–5800.
- Uchamaru, T., Stec, W. J., Tsuzuki, S., Hirose, T., Tanabe, K., and Taira, K. (1996) Ab initio investigation on nucleophilic ring opening of 1,3,2-oxathiaphosphorane: Nucleophilic substitution at phosphorus coupled with pseudorotation, *Chem. Phys. Lett.* 263, 691–696.
- Scott, W. G., Murray, J. B., Arnold, J. R. P., Stoddard, B. L., and Klug, A. (1996) Capturing the structure of a catalytic RNA intermediate: The hammerhead ribozyme, *Science* 274, 2065–2069.
- Walter, N. G., and Burke, J. M. (1998) The hairpin ribozyme: Structure, assembly and catalysis, *Curr. Opin. Chem. Biol.* 2, 24–30.
- Rupert, P. B., Massey, A. P., Sigurdsson, S. T., and Ferré-D'Amaré, A. R. (2002) Transition State Stabilization by a Catalytic RNA, *Science* 298, 1421–1424.
- Ke, A., Zhou, K., Ding, F., Cate, J. H. D., and Doudna, J. A. (2004) A conformational switch controls hepatitis delta virus ribozyme catalysis, *Nature* 429, 201–205.
- Das, S., and Piccirilli, J. (2005) General acid catalysis by the hepatitis delta virus ribozyme, *Nat. Chem. Biol.* 1 (1), 45–52.
- Truhlar, D. G., Gao, J., Garcia-Viloca, M., Alhambra, C., Corchado, J., Sanchez, M. L., and Poulsen, T. D. (2004) Ensemble-averaged variational transition state theory with optimized multidimensional tunneling for enzyme kinetics and other condensed-phase reactions, *Int. J. Quantum Chem.* 100, 1136–1152.
- Saunders, M., Laidig, K. E., and Wolfsberg, M. (1989) Theoretical Calculation of Equilibrium Isotope Effects Using ab Initio Force Constants: Application to NMR Isotopic Perturbation Studies, *J. Am. Chem. Soc.* 111, 8989–8994.
- Barnes, J. A., and Williams, I. H. (1996) Theoretical modelling of kinetic isotope effects for glycoside hydrolysis in aqueous solution by a hybrid quantum-mechanical/molecular-mechanical method, *Chem. Commun.*, 193–194.

47. Rodriguez, C. F., and Williams, I. H. (1997) Ab initio theoretical investigation of the mechanism for α -lactone formation from α -halocarboxylates: Leaving group, substituent, solvent and isotope effects, *J. Chem. Soc. Perkin Trans. 2*, 959–965.
48. Alhambra, C., Carochado, J., Sánchez, M. L., Garcia-Viloca, M., Gao, J., and Truhlar, D. G. (2001) Canonical variational theory for enzyme kinetics with the protein mean force and multidimensional quantum mechanical tunneling dynamics. Theory and application to liver alcohol dehydrogenase, *J. Phys. Chem. B* 105, 11326–11340.
49. Gao, J., and Truhlar, D. G. (2002) Quantum Mechanical Methods for Enzyme Kinetics, *Annu. Rev. Phys. Chem.* 53, 467–505.
50. Houk, K. N., Gustafson, S. M., and Black, K. A. (1992) Theoretical secondary kinetic isotope effects and the interpretation of transition state geometries. I. The Cope rearrangement, *J. Am. Chem. Soc.* 114, 8565–8572.
51. Wiest, O., Houk, K. N., Black, K. A., and Thomas, B., IV (1995) Secondary Kinetic Isotope Effects of Diastereotopic Protons in Pericyclic Reactions: A New Mechanistic Probe, *J. Am. Chem. Soc.* 117, 8594–8599.
52. Gregersen, B. A., Lopez, X., and York, D. M. (2004) Hybrid QM/MM Study of Thio Effects in Transphosphorylation Reactions: The Role of Solvation, *J. Am. Chem. Soc.* 126, 7504–7513.
53. Becke, A. D. (1993) Density-functional thermochemistry. III. The role of exact exchange, *J. Chem. Phys.* 98 (7), 5648–5652.
54. Lee, C., Yang, W., and Parr, R. G. (1998) Development of the Colle-Savettii correlation energy formula into a functional of the electron density, *Phys. Rev. B* 37, 785–789.
55. Reed, A. E., Weinstock, R. B., and Weinhold, F. (1985) Natural population analysis, *J. Chem. Phys.* 83, 735–746.
56. Range, K., McGrath, M. J., Lopez, X., and York, D. M. (2004) The Structure and Stability of Biological Metaphosphate, Phosphate, and Phosphorane Compounds in the Gas Phase and in Solution, *J. Am. Chem. Soc.* 126, 1654–1665.
57. Mayaan, E., Range, K., and York, D. M. (2004) Structure and binding of Mg(II) ions and di-metal bridge complexes with biological phosphates and phosphoranes, *J. Biol. Inorg. Chem.* 9 (7), 807–817.
58. López, C. S., Faza, O. N., de Lera, A. R., and York, D. M. (2005) Pseudorotation Barriers of Biological Oxyphosphoranes: A Challenge for Simulations of Ribozyme Catalysis, *Chem.—Eur. J.* 11, 2081–2093.
59. Tomasi, J., and Persico, M. (1994) Molecular interaction in solution: An overview of methods based on continuous distributions of the solvent, *Chem. Rev.* 94, 2027–2094.
60. Cossi, M., Scalmani, G., Rega, N., and Barone, V. (2002) New developments in the polarizable continuum model for quantum mechanical and classical calculations on molecules in solution, *J. Chem. Phys.* 117, 43–54.
61. Barone, V., Cossi, M., and Tomasi, J. (1997) A new definition of cavities for the computation of solvation free energies by the polarizable continuum model, *J. Chem. Phys.* 107 (8), 3210–3221.
62. Peng, C., Ayala, P. Y., Schlegel, H. B., and Frisch, M. J. (1996) Using redundant internal coordinates to optimize equilibrium geometries and transition states, *J. Comput. Chem.* 17, 49–56.
63. Bauernschmitt, R., and Ahlrichs, R. (1996) Stability analysis for solutions of the closed shell Kohn Sham equation, *J. Chem. Phys.* 104, 9047–9052.
64. Seeger, R., and Pople, J. A. (1977) Self-consistent molecular orbital methods. XVIII. Constraints and stability in Hartree–Fock theory, *J. Chem. Phys.* 66 (7), 3045–3050.
65. Cramer, C. J. (2002) *Essentials of Computational Chemistry: Theories and Models*, 2nd ed., John Wiley & Sons, Chichester, England.
66. Frisch, M. J., Trucks, G. W., Schlegel, H. B., Scuseria, G. E., Robb, M. A., Cheeseman, J. R., Montgomery, J. A., Jr., Vreven, T., Kudin, K. N., Burant, J. C., Millam, J. M., Iyengar, S. S., Tomasi, J., Barone, V., Mennucci, B., Cossi, M., Scalmani, G., Rega, N., Petersson, G. A., Nakatsuji, H., Hada, M., Ehara, M., Toyota, K., Fukuda, R., Hasegawa, J., Ishida, M., Nakajima, T., Honda, Y., Kitao, O., Nakai, H., Klene, M., Li, X., Knox, J. E., Hratchian, H. P., Cross, J. B., Bakken, V., Adamo, C., Jaramillo, J., Gomperts, R., Stratmann, R. E., Yazyev, O., Austin, A. J., Cammi, R., Pomelli, C., Ochterski, J. W., Ayala, P. Y., Morokuma, K., Voth, G. A., Salvador, P., Dannenberg, J. J., Zakrzewski, V. G., Dapprich, S., Daniels, A. D., Strain, M. C., Farkas, O., Malick, D. K., Rabuck, A. D., Raghavachari, K., Foresman, J. B., Ortiz, J. V., Cui, Q., Baboul, A. G., Clifford, S., Cioslowski, J., Stefanov, B. B., Liu, G., Liashenko, A., Piskorz, P., Komaromi, I., Martin, R. L., Fox, D. J., Keith, T., Al-Laham, M. A., Peng, C. Y., Nanayakkara, A., Challacombe, M., Gill, P. M. W., Johnson, B., Chen, W., Wong, M. W., Gonzalez, C., and Pople, J. A. (2004) *Gaussian 03*, revision C.02, Gaussian, Inc., Wallingford, CT.
67. Weston, R. E., Jr., and Schwarz, H. A. (1972) *Chemical Kinetics*, Prentice-Hall, Englewood Cliffs, NJ.
68. Corchado, J. C., Chuang, Y.-Y., Fast, P. L., Hu, W.-P., Liu, Y.-P., Lynch, G. C., Nguyen, K. A., Jackels, C. F., Ramos, A. F., Ellingson, B. A., Lynch, B. J., Melissas, V. S., Villa, J., Rossi, I., Coitino, E. L., Pu, J., Albu, T. V., Steckler, R., Garrett, B. C., Isaacson, A. D., and Truhlar, D. G. (2005) *POLYRATE*, version 9.3.1, University of Minnesota, Minneapolis, MN.
69. Saunders, W. H., Jr. (1980) *Investigations of Rates and Mechanisms of Reactions*, Vol. 6, pp 565–611, Wiley-Interscience, New York.
70. Bigeleisen, J., and Mayer, M. G. (1947) Calculation of Equilibrium Constants for Isotopic Exchange Reactions, *J. Chem. Phys.* 15 (5), 261–267.
71. Warshel, A., and Levitt, M. (1976) Theoretical studies of enzymatic reactions: Dielectric electrostatic and steric stabilization in the reaction of lysozyme, *J. Mol. Biol.* 103, 227–249.
72. Gao, J. (2003) Catalysis by enzyme conformational change as illustrated by orotidine 5′-monophosphate decarboxylase, *Curr. Opin. Struct. Biol.* 13, 184–192.
73. Nam, K., Gao, J., and York, D. M. (2005) An Efficient Linear-Scaling Ewald Method for Long-Range Electrostatic Interactions in Combined QM/MM Calculations, *J. Chem. Theory Comput.* 1 (1), 2–13.
74. Truhlar, D. G., and Garrett, B. C. (1984) Variational transition state theory, *Annu. Rev. Phys. Chem.* 35, 159–189.
75. Lide, D. R., Ed. (2003) *CRC Handbook of Chemistry and Physics*, 83rd ed., CRC Press, Boca Raton, FL.
76. Liu, X., and Reese, C. B. (1995) Uridylyl-(3′→5′)-(5′-thiouridine). An exceptionally base-labile di-ribonucleoside phosphate analogue, *Tetrahedron Lett.* 36 (19), 3413–3416.
77. Thomson, J. B., Patel, B. K., Jiménez, V., Eckart, K., and Eckstein, F. (1996) Synthesis and properties of diuridine phosphate analogues containing thio and amino modifications, *J. Org. Chem.* 61, 6273–6281.
78. Dantzman, C. L., and Kiessling, L. L. (1996) Reactivity of a 20-thio nucleotide analog, *J. Am. Chem. Soc.* 118, 11715–11719.
79. Liu, X., and Reese, C. B. (1996) 3′-Thiouridylyl-(3′→5′)-uridine, *Tetrahedron Lett.* 37 (6), 925–928.
80. Weinstein, L. B., Earnshaw, D. J., Cosstick, R., and Cech, T. R. (1996) Synthesis and characterization of an RNA dinucleotide containing a 30-S-phosphorothioate linkage, *J. Am. Chem. Soc.* 118 (43), 10341–10350.
81. Burgers, P. M. J., and Eckstein, F. (1979) Diastereomers of 5′-O-Adenosyl 3′-O-Uridyl Phosphorothioate: Chemical Synthesis and Enzymatic Properties, *Biochemistry* 18, 592–596.
82. Almer, H., and Strömberg, R. (1991) Intramolecular transesterification in thiophosphate-analogues of an RNA-dimer, *Tetrahedron Lett.* 32 (30), 3723–3726.
83. Almer, H., and Strömberg, R. (1996) Base catalysis and leaving group dependence in intramolecular alcoholysis of uridine 30-(aryl phosphorothioate)s, *J. Am. Chem. Soc.* 118, 7921–7928.
84. Ora, M., Oivanen, M., and Lönnberg, H. (1996) Hydrolysis and Desulfurization of the Diastereomeric Phosphoromonothioate Analogs of Uridine 20,30-Cyclic Monophosphate, *J. Org. Chem.* 61, 3951–3955.
85. Ora, M., Oivanen, M., and Lönnberg, H. (1997) Phosphoester Hydrolysis and Intramolecular Transesterification of Ribonucleoside 20- and 30-Phosphoromonothioate Triesters: Kinetics and Mechanisms for the Reactions of 50-O-Methyluridine 20- and 30-Dimethylphosphoromonothioates, *J. Org. Chem.* 62, 3246–3253.
86. Ora, M., Järvi, J., Oivanen, M., and Lönnberg, H. (2000) Hydrolytic Reactions of the Phosphorodithioate Analogue of Uridylyl(30,50)uridine: Kinetics and Mechanisms for the Cleavage, Desulfurization, and Isomerization of the Internucleosidic Linkage, *J. Org. Chem.* 65, 2651–2657.
87. Oivanen, M., Ora, M., Almer, H., Strömberg, R., and Lönnberg, H. (1995) Hydrolytic reactions of the diastereomeric phosphoromonothioate analogs of uridylyl(3′,5′)uridine: Kinetics and

- mechanisms for desulfurization, phosphoester hydrolysis, and transesterification to the 2',5'-isomers, *J. Org. Chem.* 60, 5620–5627.
88. Nielsen, J., Brill, W. K.-D., and Caruthers, M. H. (1988) Synthesis and characterization of dinucleoside phosphorodithioates, *Tetrahedron Lett.* 29 (24), 2911–2914.
89. Petersen, K. H., and Nielsen, J. (1990) Chemical synthesis of dimer ribonucleotides containing internucleotidic phosphorodithioate linkages, *Tetrahedron Lett.* 31 (6), 911–914.
90. Gerratana, B., Sowa, G. A., and Cleland, W. W. (2000) Characterization of the transition-state structures and mechanisms for the isomerization and cleavage reactions of uridine 30-*m*-nitrobenzyl phosphate, *J. Am. Chem. Soc.* 122 (51), 12615–12621.
91. Cassano, A. G., Anderson, V. E., and Harris, M. E. (2002) Evidence for Direct Attack by Hydroxide in Phosphodiester Hydrolysis, *J. Am. Chem. Soc.* 124, 10964–10965.
92. Hogg, J. L., Rodgers, J., Kovach, I. M., and Schowen, R. L. (1980) Kinetic Isotope-Effect Probes of Transition-State Structure. Vibrational Analysis of Model Transition States for Carbonyl Addition, *J. Am. Chem. Soc.* 102, 79–85.
93. Paneth, P., and O'Leary, M. H. (1991) Nitrogen and Deuterium Isotope Effects on Quaternization of *N,N*-Dimethyl-*p*-toluidine, *J. Am. Chem. Soc.* 113, 1691–1693.
94. Catrina, I. E., and Hengge, A. C. (2003) Comparisons of Phosphorothioate with Phosphate Transfer Reactions for a Monoester, Diester, and Triester: Isotope Effect Studies, *J. Am. Chem. Soc.* 125, 7546–7552.
95. Catrina, I. E., and Hengge, A. C. (1999) Comparisons of phosphorothioate and phosphate monoester transfer reactions: Activation parameters, solvent effects, and the effect of metal ions, *J. Am. Chem. Soc.* 121, 2156–2163.
96. Purcell, J., and Hengge, A. C. (2005) The Thermodynamics of Phosphate versus Phosphorothioate Ester Hydrolysis, *J. Org. Chem.* 70, 8437–8442.

BI060869F